5-2022

Chandra Spectral Constraints of the Low-metallicity Collision Ring Cartwheel Galaxy

Chloë Benton
University of Arkansas, Fayetteville

Chandra Spectral Constraints of the Low-metallicity Collision Ring Cartwheel Galaxy

An Honors Thesis submitted in partial fulfillment of the requirements

of Honors Studies in Physics

By

Chloë Benton

Spring 2022

Physics

J. William Fulbright College of Arts and Sciences

The University of Arkansas

Acknowledgments

I would like to give thanks to Dr. Bret Lehmer for giving me the chance to join his undergraduate research group as well as take on this project for my thesis. It is no small task being an undergraduate thesis advisor and I greatly appreciate the extensive and continuous insight, understanding, mentoring, and conversations we had about astrophysics and more. I have been able to grow as a researcher thanks to Dr. Lehmer's advice and support throughout the duration of this project.

I would also like to thank the Department of Physics at the University of Arkansas for awarding me the F.T. Chan and Kaiyuan Chen Endowed Research Scholarship as funding for my thesis research. Similarly, I thank the Arkansas Louis Stokes Alliance for Minority Participation (ARK-LSAMP) program for supporting this project as well as my entire undergraduate career.

Lastly, I would like to thank the rest of the undergraduate students working in Dr. Lehmer's group currently. Through this experience, I have realized that research is a collaborative effort to genuinely understand science and ultimately contribute to the greater knowledge in said community.

Thank you to the committee members for giving me their time for my defense.

Table of Contents

Abstract

With the sophistication of the Chandra X-Ray Observatory, many observations of the behaviors of binary systems have been researched and studied. As an excellent example, for the low metallicity Cartwheel Galaxy, some fraction of the X-ray photons emitted from X-ray binaries have been intercepted by the detectors on the telescope and have been compiled into “events file.” When modeled properly, this data can produce insight into the behavior of the stellar populations in this object. The primary goal of this project is to use these events files to measure the X-ray properties of the X-ray binaries in the Cartwheel Galaxy because the formation rate of these binaries is expected to be contingent on both metallicity and stellar age. Furthermore, the Cartwheel Galaxy is a collisional ring galaxy that recently underwent a burst of star formation from the collision. So, by creating Chandra data products, they can aid in the understanding of whether the X-ray emission from the X-ray binaries formed following the burst in the Cartwheel Galaxy is consistent or varying from the behavior of other galaxies.

Keywords: x-ray binary stars; metallicity; fitting techniques; emissions; spectral energy distributions

Introduction

X-ray binary systems (XRBs) are a class of binary stars that are X-ray luminous. These systems are produced by matter falling from a normal star called the donor star, to a compact object, a companion star, such as a neutron star or a black hole, called the accretor. As the matter from the donor star falls into the companion star (either through mass transfer or stellar wind capture), it releases strong gravitational potential energy in the form of X-rays, consequently the name X-ray binaries. Specifically, the Cartwheel Galaxy has many x-ray binary populations throughout the inner and outer rings.

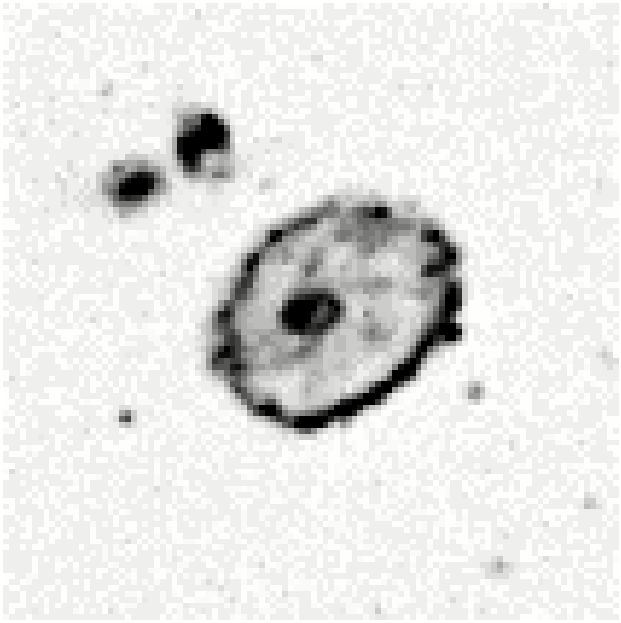

Figure 1. *Courtesy of https://ned.ipac.caltech.edu/byname?objname=Cartwheel+Galaxy&hconst=67.8&omegam=0.308&omegav=0.692&wmap=4&corr_z=1. An optical image of the Cartwheel Galaxy in the spectral band IIIaJ was taken by the telescope UK Schmidt.*

The study of XRB populations is critical, in part, due to the scalings between the X-ray luminosity of XRBs and host galaxy properties such as star formation rate (SFR), stellar mass, and metallicity. SFR is defined as the total mass of stars formed per year, frequently

given in units of solar masses per year. Metallicity is defined as the abundance of elements present in stellar objects that are heavier than hydrogen and helium. The Cartwheel Galaxy's distance, SFR, and metallicity are d = 4.629e26 cm, 18 $M_\odot\ yr^{-1}$ and Z = 0.3 $Z_\odot$ (Prestwich et al., 2012) respectively; indicating the galaxy is actively forming new stars with relatively pure gas that has not been drastically enriched by previous generations of stars. From these studies, the knowledge of the behavior of high-mass (HMXBs) and low-mass x-ray binaries (LMXBs) has been developed. High mass donor stars are in the range of $M \gtrsim 2\ M_\odot$ and are usually an O or B star, a blue supergiant, or in some cases, a red supergiant. Low mass donor stars are $M \leq 2\ M_\odot$ and tend to be either on the main sequence, a white dwarf, or a red giant. In particular, the galaxy integrated emission from HMXBs, systems with massive donor stars, tend to scale with SFR while LMXBs scale with stellar mass. In other words, the high-mass donor stars in HMXBs die off quicker following continuous star-formation events, while low-mass donors in LMXBs continue to live for billions of years since the timescale grows with declining mass. The significance of these scalings is they aid in the explanation of the stellar evolution of these binary systems and their effects, galaxy wide. As well as the evolution of the integrated x-ray emissions and spectral energy distribution over periods.

Importantly, another finding showed that, in particular cases, metallicity is likely dependent on the x-ray luminosity function, Lx, per unit SFR. Specifically, Lx/SFR increases with decreasing metallicity. (Garofali et al., 2020) This correlation is crucial since the Cartwheel Galaxy is a low-metallicity galaxy (0.3 Z). The correlation originates from the effects of metallicity on binary evolution, specifically, low metallicity systems produce more massive black holes and compact binary systems. (Garofali et al., 2020) This results in brighter XRBs, at lower metallicities i.e., the Cartwheel Galaxy which holds many

ultraluminous x-ray binaries (ULXs). (Prestwich et al., 2012) The production of the ULXs is primarily due to the head-on collision the Cartwheel had with another smaller galaxy millions of years before Chandra's observations. Through this collision, the force caused a gravitational shock wave to expand throughout the galaxy collecting gas and dust in its path. This is the culprit for the continuous starburst around the center portion of the galaxy and the outer ring. Recent starbursts due to the compression waves of expansion have lit up the outer ring of the galaxy. The star formation due to starburst results in the formation of extremely large and luminous stars such as ULXs. Furthermore, galaxies with a similar structure to the Cartwheel and hold numerous ULXs (like NGC922) are observed using restricted-energy bands which specifically target bright point-source populations. For example, the NGC922's brightest source has a band of 0.3–8.0 KeV. (Prestwich et al., 2012) Therefore, when observing these low-metallicity objects, a specific energy band is needed for the x-ray spectral energy distributions (SED). This is the reasoning for the energy band 0.5–8.0 KeV used throughout this project since it is comparable to other low-metallicity, star-forming galaxies. In analyzing the SEDs for the Cartwheel Galaxy, a general model can be constructed for similar behaving galaxies.

Observations and Data Analysis

In this section, I present and analyze three observations from Chandra of the Cartwheel Galaxy through software-generated images and spectra as well as an overview of the data reduction process used.

Chandra Imaging and Spectra

The Chandra X-ray Observatory was launched in 1999 and until currently, has taken many observations. Specifically, I analyzed three different observations taken at various times. The first observation, the **2019** epoch, was observed in 2001 and had the longest exposure time, 76.1 ks. The second and third observations, **9531** and **9807** epochs were observed in 2008, and both had similar exposure times, ~45 ks. See **Table 1**. I also analyzed another data file, **stacked**, which is a file compiled of the three epochs, and used it as a base model to compare the other epochs.

Before the analysis and modeling could begin, specific software and its environment `CIAO` version 4.13 had to be installed onto my computer for the data sets to be processed correctly. Within the `CIAO` environment, there are two important packages `SHERPA` and `DS9` which allow for spectra modeling and image inspection, respectively. Specifically, for these data sets, it is crucial that every product is scaled using a logarithmic scale. The reasoning behind this is the relationships within the data sets are modeled using a power-law model.

Then being able to analyze data within the `CIAO` environment, I ran the following strip of code to produce images of the Cartwheel Galaxy through various epochs or observations:

$$ds9\ -\log */*\ -best.evt2\ \&$$

The `-log` is needed so the image is automatically scaled with log when the image is created. The $*/*$ is a placeholder for the name of a specific events file that I wanted to generate. The spectra files of interest for this project were 2019-best.evt2, 9531-best.evt2, 9807-best.evt2, and a stacked file with all the data co-added. Another note to make is the number

designations in the file names are important because the first number denotes the observation taken by Chandra. So, the event file of 2019 occurred during the second year of Chandra operations while the event files of 9531 and 9807 occurred during the ninth year.

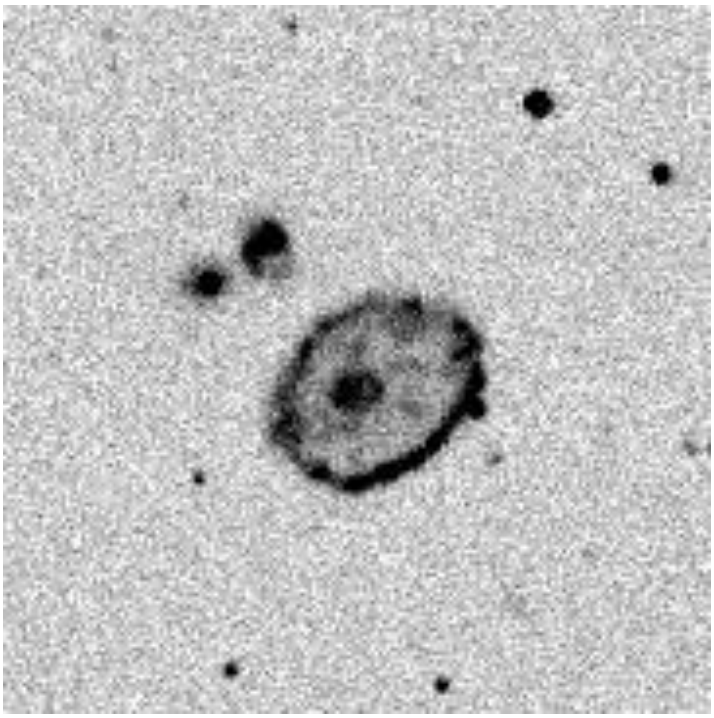

Figure 2*. Courtesy of https://ned.ipac.caltech.edu/byname?objname= Cartwheel+Galaxy&hconst=67.8&omegam=0.308&omegav=0.692&wmap=4&corr_z=1. Optical image of the Cartwheel Galaxy in the spectral band B taken by the telescope ESO1m. The orientation is a standard for the following images.*

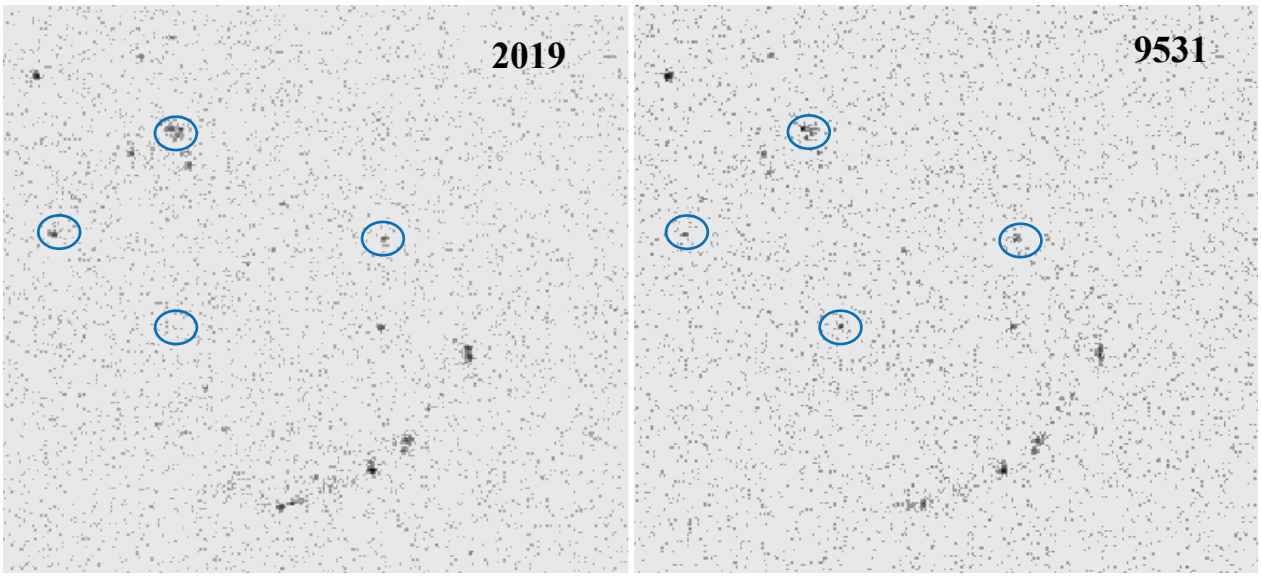

Figure 3. *Image generated through ds9 software of the 2019 and 9531 epochs. Dark black regions are areas of expected point sources detected from the XRB component.*

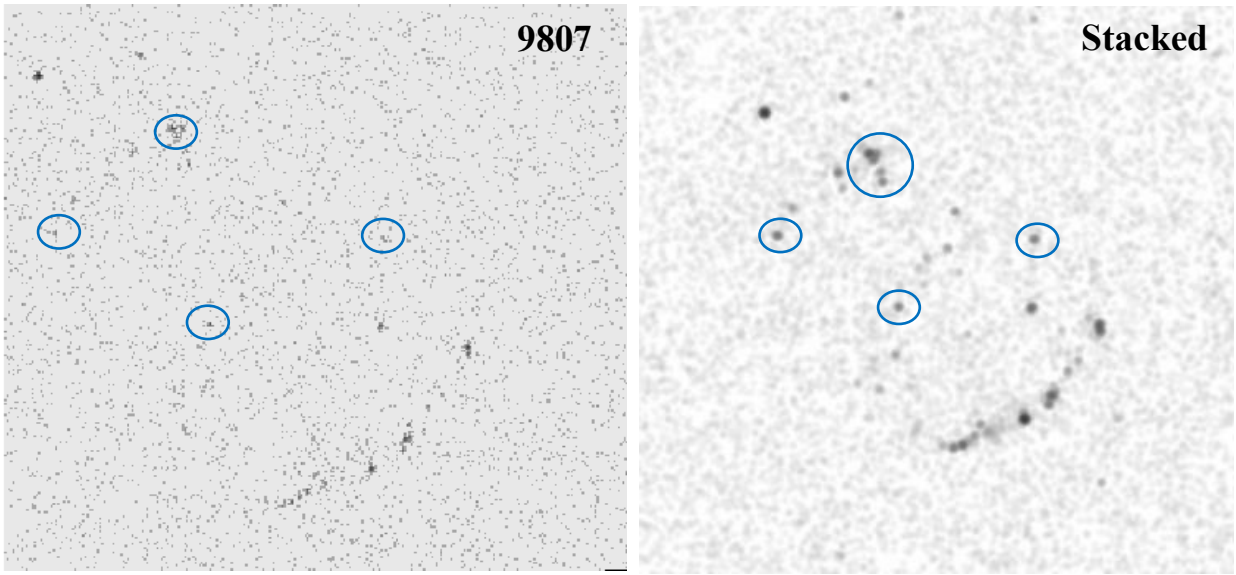

Figure 4. *Image generated through ds9 software of the 9807 epoch and stacked. Dark black regions are the areas of expected point sources detected that have either turned off, lit up, or remained the same from the previous observations.*

The darker regions are likely to be XRBs activity. A note to make is the images are zoomed in to focus on the galaxy and ignore outside bright sources that are likely not a part of the galaxy. These assumptions are made due to the fact that we know the Cartwheel Galaxy is structured in rings. It has two rings, a large outer ring and then a smaller inside ring. See **Fig 2.** So, any sources that are outside of the outer ring are attributed to background sources (e.g., distant active galactic nuclei). The images have also been inverted in color so the point sources can be easily identified. Throughout the different images, there are quite a few notable differences (circled regions). See **Figs 3-4**. Some regions have been added due to them either appearing brighter than before or turning on, i.e., star-formation. It appears that some regions have also disappeared due to dimming or turning off completely, this is emphasized when comparing **9807** to **2019**. Since **9807** is in the same observation period as **9531**, I would not have expected such a noticeable difference between the two, but the culprit could be the photon and detector interaction, i.e., energy leaks. Especially since the counts for **9807** were the lowest amongst all four data sets. See **Table 1** for more information. The last image is a model of what the Cartwheel Galaxy would appear as when all the epochs are overlayed into one image. As expected, since there are many dark regions, this data set had the most source and background counts “detected.”

Table 1

Data Products by Observation

Epochs (Observations)	**2019**	**9531**	**9807**	**stacked**
Total Source Counts	2948	2321	2135	7404
Source Count Rate	0.038713	0.048537	0.043109	0.042676
Total Background Counts	5675	5870	6156	17701
Background Count Rate	0.074524	0.122755	0.1243	0.102027
Observation Date	2001-05-26	2008-01-21	2008-09-09	----------
Exposure Time [ks]	76.1	48.0	49.5	----------
Unabsorbed Flux [ergs/cm^2/s]	1.29E-13	1.07E-13	7.28E-14	1.07E-13
Absorbed Flux [ergs/cm^2/s]	1.19E-13	1.07E-13	7.09E-14	1.04E-13
Unabsorbed Luminosity [ergs/s]	3.49E+41	2.87E+41	1.96E+41	2.88E+41
Absorbed Luminosity [ergs/s]	3.19E+41	2.87E+41	1.91E+41	2.80E+41
N_H [10^{21} cm^{-2}]	0.072 +/- 0.032	0 +/- 0.049	0.014 +/- 0.063	0.019 +/- 0.024
Γ	1.801 +/- 0.129	1.77 +/- 0.209	2.13 +/- 0.303	1.79 +/- 0.104
Amplitude (A_Γ)	2.523E-5 +/- 2.667E-6	2.023E-5 +/- 3.303E-6	1.787E-5 +/- 3.66E-6	2.051E-5 +/- 1.66E-6

Data Collection and Fitting Techniques

Beyond using the data sets for image comparison, the next step was to apply fitting techniques to quantitively analyze the data. The obvious and more obscured point-source regions can now have values assigned which allow for the possibility of spectra modeling. By extracting the spectral data from the .pi files (which include source and background source information), then creating diagrams that focus on the photon counts per energy (0.5-8.0 KeV) captured by Chandra, more products can then aid in the understanding of the evolution of XRB behavior.

When analyzing the data sets, it was imperative for the data to be folded and fitted through the correct models to be able to produce the most accurate distribution curves. The sources and background spectra need to have separate models that are factored in the power-law such that the full model would process accurately. The statistic used to fit the model was set to C-statistic, a Poisson probability distribution model, since a Gaussian model (such as χ^2) would not work properly for the source model **(2)**. The reason being is uncertainties arises from the application of Gaussian models, especially in spectral fitting and spectral binning. Poisson models (C-statistic) are more beneficial when it comes to data based on counts.

The background (bmdl) and source (smdl) models were constructed methodically. $xscplinear$ is a non-physical piecewise-linear model for low count background spectra and the various $xsgaussian.line\_$ accounts for the line emission parameters which can be added together since it is a component of the function. The bmdl was then scaled by the background of the data set which included the instrument response. From there it was added to

$xsphabs.abs1 * powlaw1d.p1$ to create the smdl. $xsphabs.abs1$ accounts for the photoelectric absorption (or column density) and $powlaw1d.p1$ is the power-law function.

$$bmdl = \text{“}xscplinear.bkg1 + xsgaussian.line1 + xsgaussian.line2 + xsgaussian.line3 + xsgaussian.line4 + xsgaussian.line5 + xsgaussian.line6\text{”} \quad (1)$$

$$smdl = xsphabs.abs1 * powlaw1d.p1 + scale * bmdl \quad (2)$$

Using the standard reduction tools built into CIAO, SHERPA, and custom python codes, the models were fitted, and the results were plotted. Additionally, the background spectra was extracted and then set as a stand-alone trend to be compared to the source spectra. See **Figures 5-6** for a clearer representation.

In addition to the best-fit model distributions, important variables of the power-law model were quantified: N_H, Γ, and amplitude. N_H, the column density, is defined as the number of hydrogen atoms (HI) per square cm (cm^2) projected along a particular line of sight. As seen in **Table 1**, these values are relatively low, and negligible. For reference, the column density for a comparable low-metallicity galaxy, VV114 X-1, is $N_H = 2.11^{+0.36}_{-0.23} * 10^{22}$ cm^{-2}. (Garofali et al., 2020) The Γ, the photon index, for each observation of Cartwheel is consistent with expectations for similar galaxies while the amplitudes are slightly higher. For VV114 X-1, $\Gamma = 1.01^{+0.59}_{-0.24}$ and $A_\Gamma = 0.97^{+1.24}_{-0.30} * 10^{-5}$. (Garofali et al., 2020) A note to make is since the column density modifies the model, it is understandable that the amplitude varies between observations and galaxies.

Physical Quantities

An additional technique was used to “clean up” the graphs such that the actual curves could be analyzed. This allowed for the source and background trends to be more easily visualized. Once again, the axes were scaled with log due to the models. Since the photons emitted are in the x-ray spectrum, the Chandra telescope is only able to detect photon energies between 0.5–8.0 KeV. Above that scale, the counts drop off.

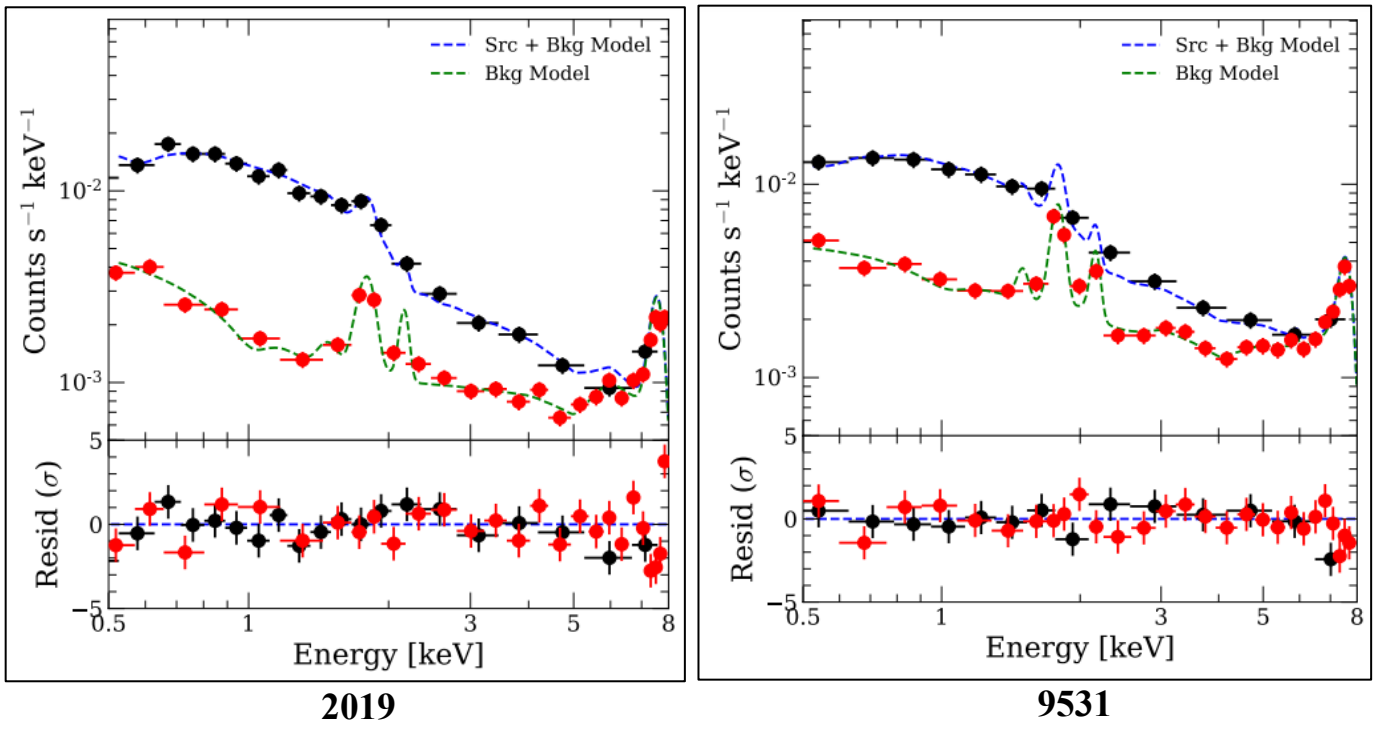

Figure 5. *The best-fit distribution models of the 2019 and 9531 data files. The curves represent best-fit models to the source (blue dashed) and background (green dashed) data containing contributions from either the XRB component and/or background sources.*

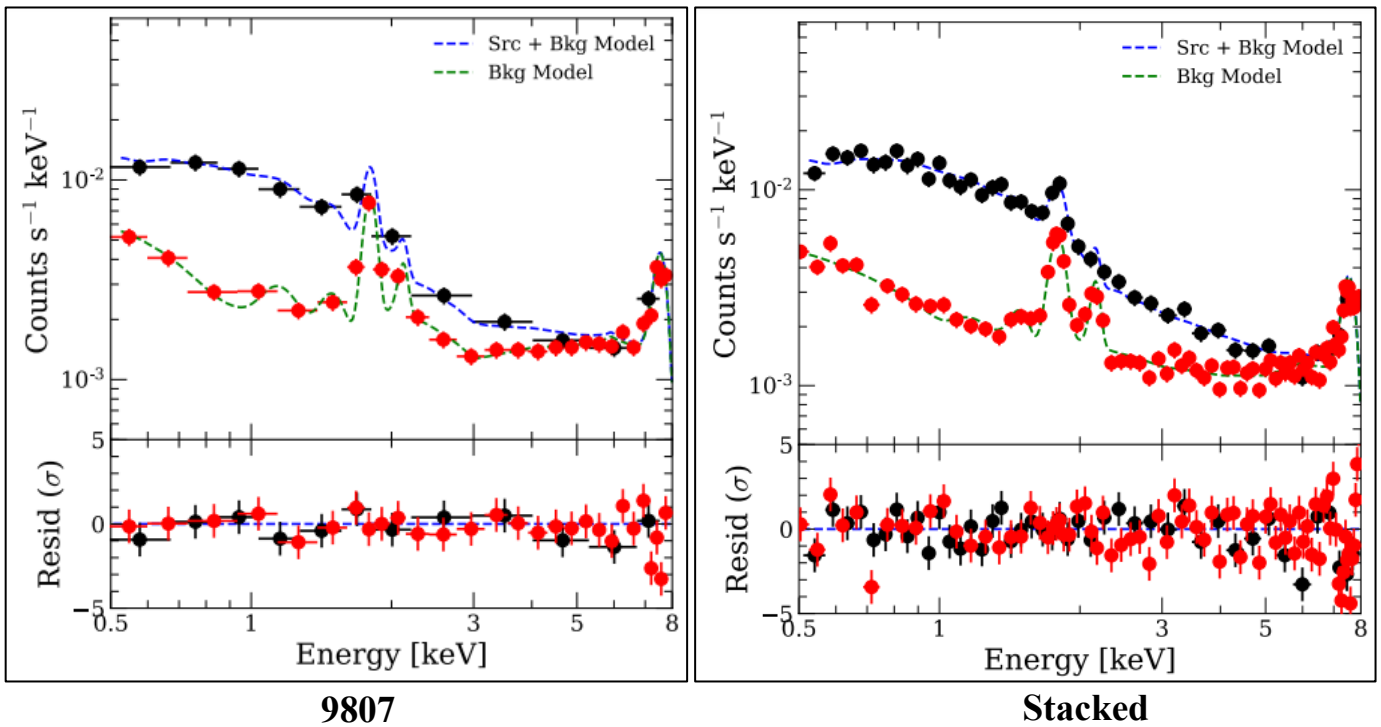

Figure 6. *The best-fit distribution model of the 9807 and stacked data file. See* ***Figure 5*** *for more information.*

The figures above demonstrate a best-fit distribution of the source and background models for each of the observations as well as the stacked file. As seen in **Figs. 3-4**, there were regions where the points were darker than the background. This is quantified in **Figs. 4-5**. The points represent photons that have been intercepted by the Chandra detectors and their specific photon energy. The points have also been binned such that 100 photons (counts) with similar energy levels were grouped to represent one dot. See **Table 1** for total counts per epoch. The purpose of filtering the data is so the background can be extracted from the point-source populations and modeled distinctly. The residuals panel is to account for sources detected that did not fit the model accurately (bad photons) or energy leaks. The lines on the points are error bars and they account for the uncertainties that follow the residuals. A note to make is that similar to the generated DS9 image of **9807**, there is less of a distinction between the background model and the total model. In the image, there were not as many evident point sources, and this reflects why the trends are overlapping (and falling off) at a faster rate towards the higher energy levels than in the other diagrams.

Additional quantities measured were the integrated 0.5–8.0 KeV flux and luminosity measured from each of the epochs and the overall luminosity and flux for the galaxy. It is interesting how the flux and luminosity varied between observations. Both quantities seem to decrease over time between each epoch with **9807** having the overall lowest quantities. This reflects the generated images since the last observation has the least amount of dark regions, least overall total source counts, but most total background sources.

Results and Discussion

To construct the galaxy-wide x-ray SED of the Cartwheel Galaxy and estimate the XRB contribution, I used the same data sets. The spectral modeling and fit approach for each observation was relatively the same process used in the previous section except for additional mathematical codes that focused on the point-source populations. In the following sections, I present the methods used for the fits as well as a comparison of results between the different epochs, and the galaxy-wide spectrum of the Cartwheel Galaxy.

The process for coding and creating the spectral energy distributions was fairly straightforward. First, I created an energy array spanned from 0.5 to 8.0 that had 1000 values to evaluate.

$$earray = np.arrange(1000)/999.* (8. - 0.5) + \ 0.5 \tag{3}$$

From there, I used the luminosity function vL_v but I needed a conversion factor q that converted my units into one more feasible for this project.

$$counts\ s^{-1} \rightarrow erg\ s^{-1}$$

$$q = 1.60218e - 9\ \ [erg/KeV] \tag{4}$$

The luminosity function requires the source model from earlier (2), the energy array (3), the conversion factor (4), and the distance to the object d_x.

$$d_x = 4.629e26\ [cm] \tag{5}$$

$$vL_v = q * (earray^2) * smdl(earray) * 4 * np.pi * d_x^2 \tag{6}$$

For the SED to be scaled correctly it also needs to be normalized by the SFR and the factor that accounts for the ultraluminous sources.

$$SFR\ =\ 18\ [M_\odot\ yr^{-1}] \tag{7}$$

$$\sim 1e39$$

So, the units of the x-axis and y-axis, respectively are…

$$[KeV]$$

$$[10^{39}\ erg\ s^{-1}\ (M_{\odot}\ yr^{-1})^{-1}]$$

From there, the plotting process was similar to that of the distribution models and the following SEDs were scaled with log.

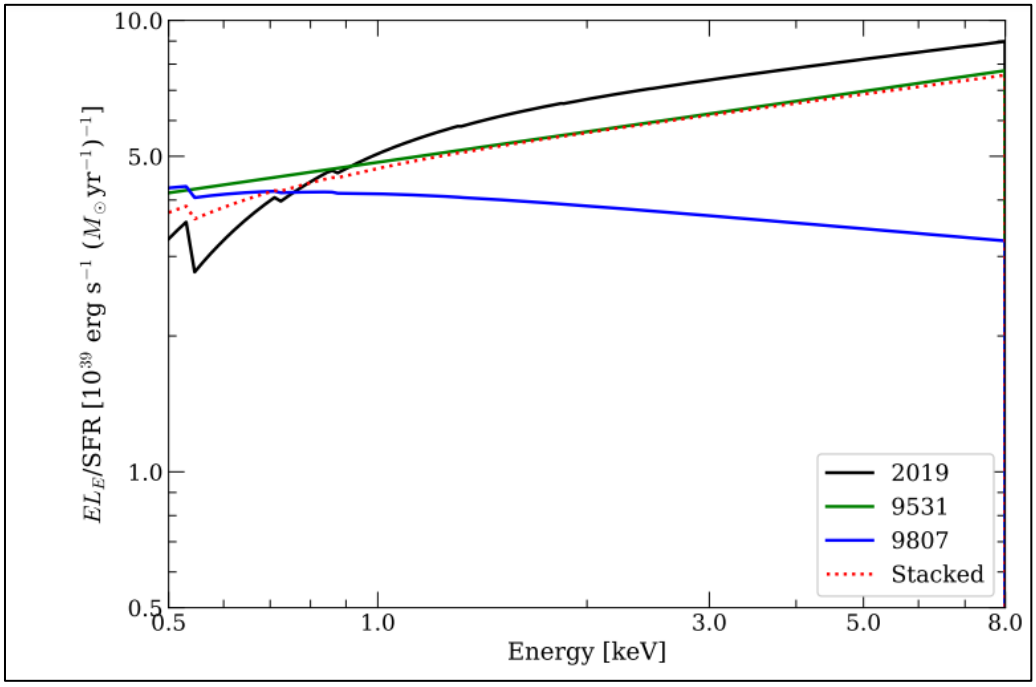

Figure 7. *The SFR-normalized 0.5–8.0 KeV SED (spectral energy distribution) model the three observations and combined "stacked" observation. The SED has been normalized by the SFR and discrete ULX) sources of the Cartwheel Galaxy (18 $M_{\odot}\ yr^{-1}$) and (10^{39} erg s^{-1}). (Prestwich et al., 2012) Displayed is the background-subtracted model focused on the XRB component, unfolded and unbinned but constrained by the [0.5-8.0] energy array.*

To put our results into context, in **Figs. 7** and **8**, presented is the best-fit spectrum for the Cartwheel, and the spectrum of several comparison galaxies from Garofali et al. (2020), respectively. We found the overall trend for the SED of the Cartwheel Galaxy is relative to the other low-metallicity galaxies. The SED also supports the initial claim that was made

about the relationship between metallicity and Lx/SFR. To demonstrate this more clearly, the following diagram has been created which overlays the SEDs of the epochs and stacked with other known SEDs of galaxies with similar and different metallicities. With the following diagram, we can gain a better understanding of how star-forming, binary populated galaxies behave and evolve and not just low-metallicity galaxies.

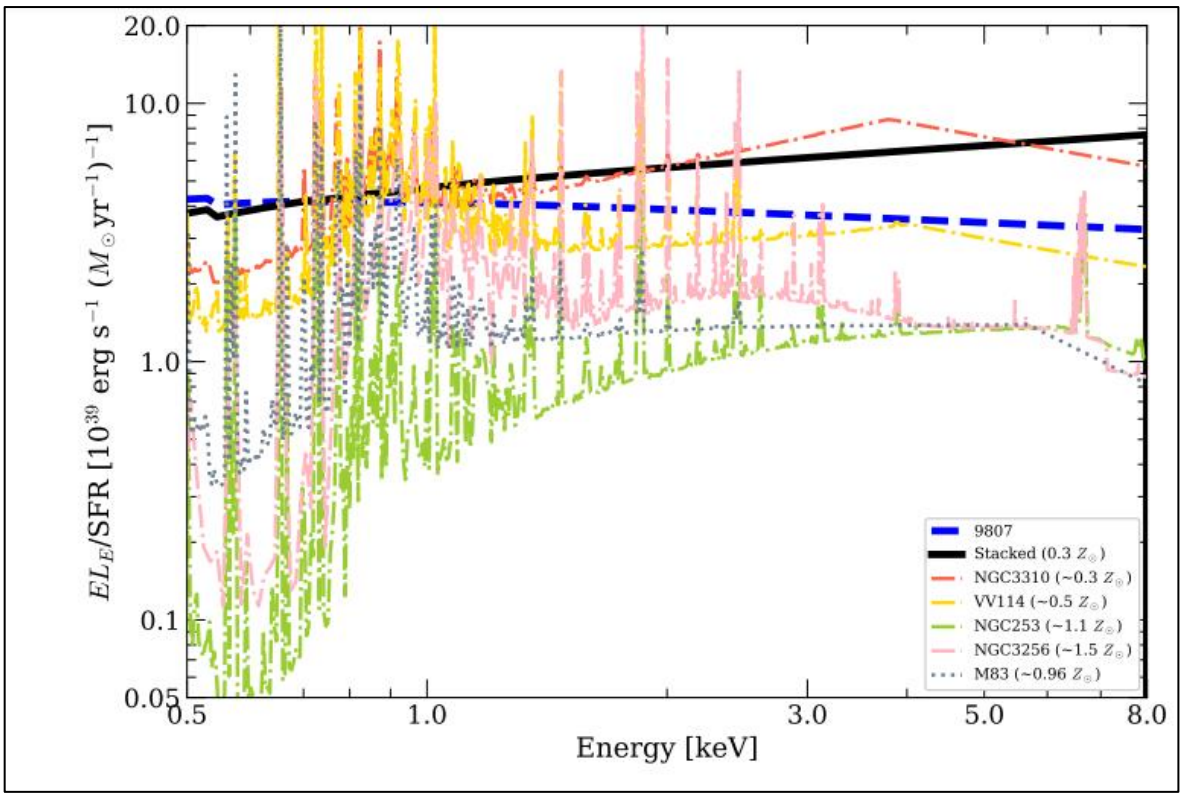

Figure 8. *Total best-fit SFR-normalized 0.5–8.0 keV SED of the Cartwheel Galaxy is displayed as a solid black line. The 9807 epoch is displayed as a dashed blue line. The observed SFR-normalized SEDs of five other star-forming galaxies at different metallicities for comparison are overlayed: NGC253 (green, ~1.1 $Z_\odot$; Garofali et al. 2020), NGC3256 (pink, ~1.5 $Z_\odot$; Garofali et al. 2020), M83 (blue, ~0.96 $Z_\odot$; Garofali et al. 2020), NGC 3310 (red, ~0.30 $Z_\odot$; Garofali et al. 2020), and VV114 (yellow; ~0.50 $Z_\odot$; Garofali et al. 2020).*

Summary and Future Works

Even though the data sets I have used have been processed and analyzed extensively, there is still much more research that can be conducted. Future works can further this project by analyzing the Cartwheel Galaxy from different angles to learn more about its behavior concerning the effects of x-ray emission on the universe. For example, it is thought that emissions from X-ray binaries could be a dominant source of heating for the intergalactic medium before the epoch of reionization (e.g., the birth of stars, galaxies, quasars, etc.). X-ray binary systems are extraordinarily complex, and it is important to understand how both high-mass and low-mass binary systems function as well as how those factors vary with the overall metallicity of the host galaxy. It is also important to analyze how x-ray binary systems change when the compact object switches from a black hole to a neutron star, particularly with galaxy evolution, star formation rate, stellar mass, stellar lifespans, etc. Further research can explore more x-ray emissions in a high redshift universe.

References

Amram, P., Mendes de Oliveira, C., Boulesteix, J., & Balkowski, C. (1998, February). The Hα kinematic of the Cartwheel galaxy. Retrieved 2021, from https://ui.adsabs.harvard.edu/abs/1998A%26A...330..881A/abstract.

Analysis guides. CIAO 4.14. (2021, October 29). Retrieved March 22, 2022, from https://cxc.harvard.edu/ciao/guides/

Garofali, K., Lehmer, B. D., Basu-Zych, A., West, L. A., Wik, D., Yukita, M., Vulic, N., Ptak, A., & Hornschemeier, A. (2020). On the X-ray spectral energy distributions of STAR-forming galaxies: The 0.3–30 kev spectrum of the low-metallicity Starburst Galaxy VV 114. The Astrophysical Journal, 903(2), 79. https://doi.org/10.3847/1538-4357/abba2d

Harvard-Smithsonian Center for Astrophysics. (n.d.). *Our Standard Chandra-Ed Observations*. Chandra-Ed Data. Retrieved April 13, 2022, from http://rinzai.rutgers.edu/archive.html#

Lee, N. P., McDowell, J. C., Tingle, E. D., & Guardado, K. M. (2011). An X-ray Data Primer. Cambridge University Press.

Mayya, Y. D., Bizyaev, D., Romano, R., Garcia-Barreto, J. A., & Vorobyov, E. I. (2005). The detection of Nonthermal Radio Continuum Spokes and the study of star formation in the cartwheel. The Astrophysical Journal, 620(1). https://doi.org/10.1086/428400

Pizzolato, F., Wolter, A., & Trinchieri, G. (2010). Chandra observations of the ULX N10 in the Cartwheel Galaxy. Monthly Notices of the Royal Astronomical Society. https://doi.org/10.1111/j.1365-2966.2010.16735.x

Prestwich, A. H., Galache, J. L., Linden, T., Kalogera, V., Zezas, A., Roberts, T. P., Kilgard, R., Wolter, A., & Trinchieri, G. (2012). Chandraobservations of the collisional ring galaxy NGC 922. The Astrophysical Journal, 747(2), 150. https://doi.org/10.1088/0004-637x/747/2/150

(n.d.). Retrieved 2022, from https://ned.ipac.caltech.edu/byname?objname=Cartwheel+Galaxy&hconst=67.8&omegam=0.308&omegav=0.692&wmap=4&corr_z=1.

Swinburne University of Technology. (n.d.). *Column density: Cosmos*. Column Density | COSMOS. Retrieved April 13, 2022, from https://astronomy.swin.edu.au/cosmos/C/Column+Density

Vorobyov, E., & Bizyaev, D. (2001). Radial $B-V/V-K$ color gradients, extinction-freeqbvkcombined color indices, and the history of star formation of the cartwheel ring galaxy. Astronomy & Astrophysics, 377(3), 835–844. https://doi.org/10.1051/0004-6361:20011163

Wolter, A., & Trinchieri, G. (2004). A thorough study of the intriguing X-ray emission from the Cartwheel Ring. Astronomy & Astrophysics, 426(3), 787–796. https://doi.org/10.1051/0004-6361:20047110

Yuan, T., Elagali, A., Labbé, I., Kacprzak, G. G., Lagos, C. del, Alcorn, L. Y., Cohn, J. H., Tran, K.-V. H., Glazebrook, K., Groves, B. A., Freeman, K. C., Spitler, L. R., Straatman, C. M., Fisher, D. B., & Sweet, S. M. (2020). A giant galaxy in the young universe with a massive ring. Nature Astronomy, 4(10), 957–964. https://doi.org/10.1038/s41550-020-1102-7